

## Bound state of an exciton-magnon system under high magnetic fields. II. $\text{YbCrO}_3$

N. Kojima

Department of Chemistry, Faculty of Science, Kyoto University, Kyoto 606, Japan

(Received 21 September 1992)

In  $\text{YbCrO}_3$ , the  $\text{Cr}^{3+}$  exciton coupled with the  $\text{Yb}^{3+}$  spin-flip state ( $R'$  band) appears on the higher-energy side of the  $\text{Cr}^{3+}$ -exciton lines corresponding to the  ${}^4A_{2g} \rightarrow {}^2E_g$  transition of  $\text{Cr}^{3+}$ . We found that a bound state appears on the lower-energy side of the  $R'$  band and has a strong dependence on external magnetic field. The bound state of the  $R'$  band changes from a localized state to a delocalized state with increasing magnetic field. In the process of the delocalization, the bound state undergoes Davydov splitting due to intersublattice migration.

### I. INTRODUCTION

In magnetic materials, the bound state of the exciton-magnon system has been observed in  $\text{MnF}_2$  (Refs. 1 and 2) and  $\text{YbCrO}_3$ .<sup>3,4</sup> In the previous paper,<sup>5</sup> we have reported the detailed behavior of the exciton-magnon bound state corresponding to the  ${}^6A_{1g} \rightarrow {}^4A_{1g}, {}^4E_g$  transition in  $\text{MnF}_2$  under high magnetic fields, and have elucidated the formation mechanism of the bound state.

Recently, we have found that a bound state appears on the lower-energy side of the  $\text{Cr}^{3+}$  exciton coupled with the  $\text{Yb}^{3+}$  spin-flip state ( $R'$  band) in  $\text{YbCrO}_3$  and has a strong dependence on external magnetic field.<sup>3,4</sup> Our main purpose in the present paper is to investigate the detailed behavior of the bound state of the  $\text{Cr}^{3+}$  exciton coupled with the  $\text{Yb}^{3+}$  spin flip and to make clear its formation mechanism.

We briefly summarize important properties of  $\text{YbCrO}_3$ . The crystal has an orthorhombically distorted perovskite structure belonging to the space group  $Pbnm$  with lattice constants  $a = 5.20 \text{ \AA}$ ,  $b = 5.51 \text{ \AA}$ , and  $c = 7.49 \text{ \AA}$  at room temperature.<sup>6</sup> The unit cell contains four molecules.<sup>6</sup> The  $\text{Cr}^{3+}$  spins are antiferromagnetically ordered below  $T_N = 118 \text{ K}$  with a weak ferromagnetic moment as  $\Gamma_2(F_x C_y G_z; F_x C_z)$  in Bertaut notation.<sup>7,8</sup> The spontane-

ous magnetic moment of  $\text{YbCrO}_3$  crosses to zero at  $16.5 \text{ K}$ , which reveals that the induced magnetic moment of the  $\text{Yb}^{3+}$  spins couples antiparallel to the weak ferromagnetic moment of the  $\text{Cr}^{3+}$  spins.<sup>7</sup> The crystal and spin structures are shown in Fig. 1. The antisymmetric (Dzyaloshinsky-Moriya) and the anisotropic-symmetric parts of the  $3d$ - $4f$  magnetic exchange interaction in  $\text{YbCrO}_3$  are enormously stronger than those in the other rare-earth orthochromites,<sup>9</sup> and these anisotropic parts of the  $3d$ - $4f$  exchange interaction induce the cooperative transition of a  $\text{Cr}^{3+}$  exciton and a  $\text{Yb}^{3+}$  spin flip.<sup>10</sup>

### II. EXPERIMENTAL PROCEDURE

The absorption spectra were measured with a Jobin Yvon model THR1500 spectrometer and an HTV R376 photomultiplier. The accuracy of this measurement was  $0.04 \text{ \AA}$  for sharp absorptions. Magnetic fields up to  $7 \text{ T}$  were produced by a Helmholtz-type superconducting magnet.

### III. EXPERIMENTAL RESULTS

Figure 2 shows the absorption spectra corresponding to the  ${}^4A_{2g} \rightarrow {}^2E_g$  transition of  $\text{Cr}^{3+}$  in  $\text{YbCrO}_3$  at  $2.0 \text{ K}$ . In the lowest-energy region, four sharp magnetic dipole lines ( $R_1, R_2, R_3$ , and  $R_4$ ) were observed. In the case of  $R_2$ , it appears only in the presence of the external magnetic field. The  $R_1$ - $R_4$  lines are the Davydov split components of the  $\text{Cr}^{3+}$  exciton corresponding to the transition from the lowest substate of  ${}^4A_{2g}$  to the lowest substate of  ${}^2E_g$  of the  $\text{Cr}^{3+}$  ion.<sup>10</sup> At the spectral position about  $90$ - $180 \text{ cm}^{-1}$  higher than the  $\text{Cr}^{3+}$ -exciton lines, very strong sidebands ( $I_A, I_B, II_A$ , and  $II_B$ ) of electric-dipole origin were observed, whose absorption coefficients are 1 or 2 orders of magnitude stronger than those of the  $\text{Cr}^{3+}$ -exciton lines. The  $I_A$  and  $I_B$  bands are considered to be the combined excitation of a  $\text{Cr}^{3+}$  exciton and a  $\text{Cr}^{3+}$  magnon on the boundary of the Brillouin zone.<sup>11</sup> In the neighborhood of the  $\text{Cr}^{3+}$ -exciton lines, an electric-dipole band ( $R'$  band) was observed, which has an anomalous shape with a sharp cutoff at the lowest-energy side and fine structure. The  $R'$  band is the excitation of the  $\text{Cr}^{3+}$  exciton coupled with  $\text{Yb}^{3+}$  spin flip.<sup>10</sup> From the analysis of the bandwidth and the energy posi-

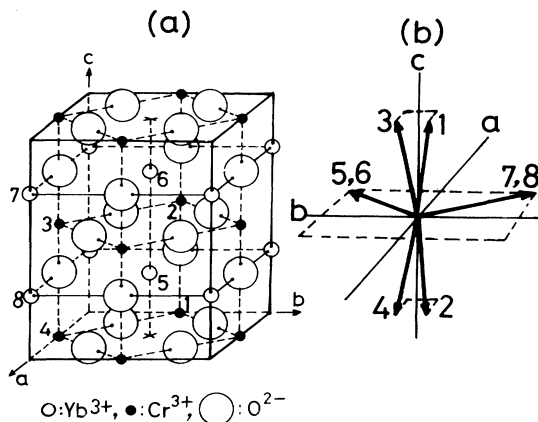


FIG. 1. (a) Unit cell of  $\text{YbCrO}_3$ . The  $\text{Cr}^{3+}$  and  $\text{Yb}^{3+}$  positions are indicated with numbers 1-4 and 5-8, respectively. (b) Spin configuration of  $\text{YbCrO}_3$  below  $T_{N1} (= 118 \text{ K})$ .

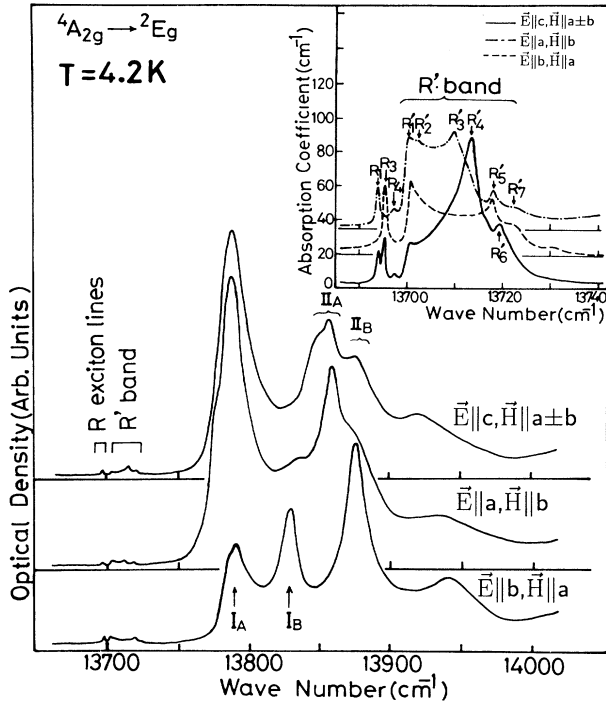


FIG. 2. Absorption spectra corresponding to the  ${}^4A_{2g} \rightarrow {}^2E_g$  transition of  $\text{Cr}^{3+}$  in  $\text{YbCrO}_3$  at 4.2 K. The inset shows the absorption spectra in the lowest-energy region of the  ${}^4A_{2g} \rightarrow {}^2E_g$  transition.  $\mathbf{E}$  and  $\mathbf{H}$  denote the electric and magnetic vectors of the incident light, respectively.

tion of the  $R'$  band, the energy dispersion of the  $\text{Cr}^{3+}$  exciton corresponding to the  ${}^4A_{2g} \rightarrow {}^2E_g$  transition is estimated to be  $-16 \text{ cm}^{-1}$ . The negative dispersion is reflected in the cutoff profile at the lowest-energy side of the  $R'$  band. That is, the low-frequency edge of the  $R'$  band corresponds to the  $\text{Cr}^{3+}$  exciton coupled with  $\text{Yb}^{3+}$  spin flip at the Brillouin zone edge. The appearance of the multiple peaks in the  $R'$  band is attributed to the Van Hove singularities in the density of the  $\text{Cr}^{3+}$ -exciton states.

As shown in Fig. 3, when the external magnetic field is applied along the  $a$  axis of  $\text{YbCrO}_3$  at 2.0 K, sharp and strong peaks (arrows in Fig. 3) typical of bound states appear on the low-frequency edge of the  $R'$  band for all the polarized lights. At about 2.5 T, where the bound states grow most strongly, the number of the bound states is two. Above 3.0 T, the bound states split into seven peaks and their intensities decrease significantly for the polarized lights of  $\mathbf{E}||\mathbf{b}$  and  $\mathbf{E}||\mathbf{c}$ . At about 6.7 T, a dramatic spectral change occurs for all the polarized lights.

Figure 4 shows the detailed behavior of the  $R'$  band in the vicinity of 6.7 T. The discontinuous spectral change at 6.7 T is due to the metamagnetic phase transition where the weak ferromagnetic moment of the  $\text{Cr}^{3+}$  spins reverses its direction from being antiparallel to parallel to the net magnetic moment of the  $\text{Yb}^{3+}$  spins.<sup>12</sup> At this metamagnetic transition, the profile of the  $R'$  band changes drastically and its bound state disappears completely. The profiles of the  $R'$  band for  $\mathbf{E}||\mathbf{a}$ ,  $\mathbf{b}$ , and  $\mathbf{c}$  are different from one another below 6.7 T. On the contrary,

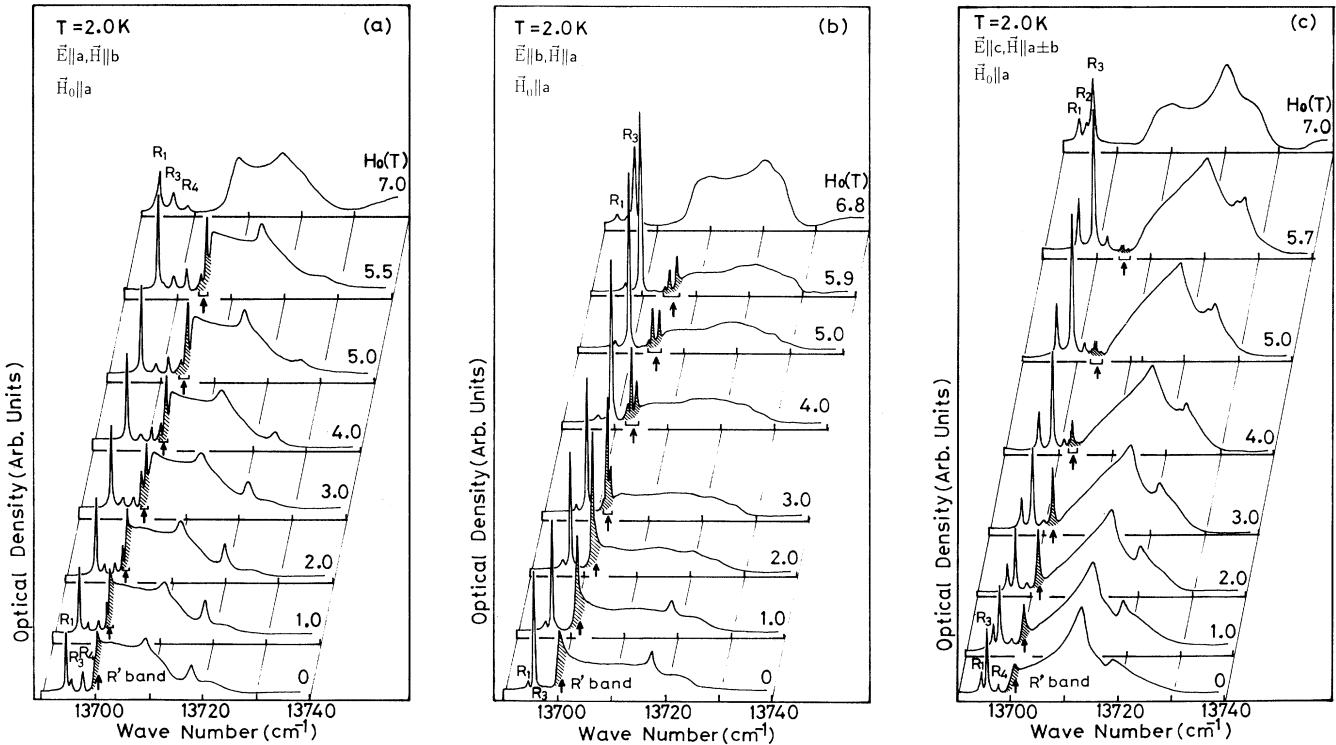


FIG. 3. Magnetic field dependence of the absorption spectra corresponding to the lowest-energy region of the  ${}^4A_{2g} \rightarrow {}^2E_g$  transition of  $\text{Cr}^{3+}$  in  $\text{YbCrO}_3$  at 2.0 K. Arrow shows the bound state of the  $R'$  band. The magnetic field  $\mathbf{H}_0||\mathbf{a}$ . (a)  $\mathbf{E}||\mathbf{a}$ ,  $\mathbf{H}||\mathbf{b}$ . (b)  $\mathbf{E}||\mathbf{b}$ ,  $\mathbf{H}||\mathbf{a}$ . (c)  $\mathbf{E}||\mathbf{c}$ ,  $\mathbf{H}||\mathbf{a} \pm \mathbf{b}$ .

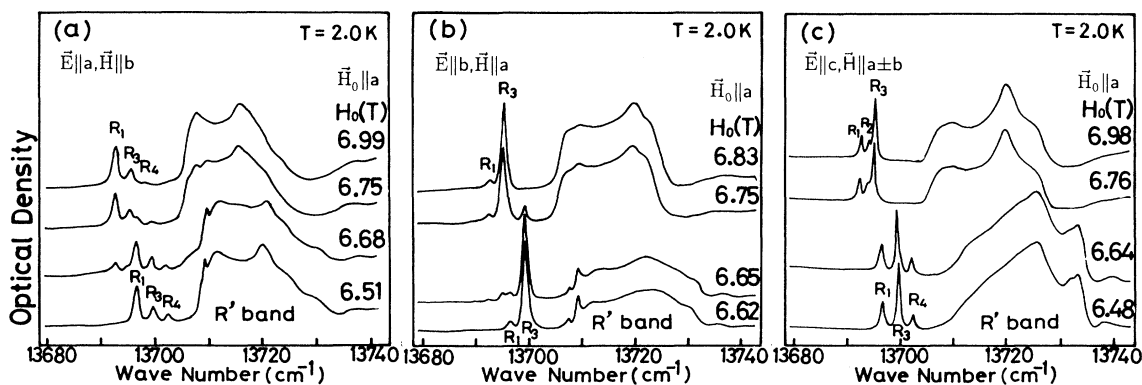


FIG. 4. Behavior of the  $R$  lines and  $R'$  band in  $\text{YbCrO}_3$  near 6.7 T at 2.0 K. The magnetic field  $\mathbf{H}_0 \parallel \mathbf{a}$ . (a)  $\mathbf{E} \parallel \mathbf{a}$ ,  $\mathbf{H} \parallel \mathbf{b}$ . (b)  $\mathbf{E} \parallel \mathbf{b}$ ,  $\mathbf{H} \parallel \mathbf{a}$ . (c)  $\mathbf{E} \parallel \mathbf{c}$ ,  $\mathbf{H} \parallel \mathbf{a} \pm \mathbf{b}$ .

these profiles of the  $R'$  band are very similar to one another above 6.7 T.

Figure 5 shows the behavior of the  $R'$  band under high magnetic fields along the  $a$  axis.<sup>11</sup> In the range of the magnetic field where the energy position of the  $R'$  band approaches that of the  $\text{Cr}^{3+}$ -exciton- $\text{Cr}^{3+}$ -magnon transition ( $I_A$  and  $I_B$  bands), the intensity of the  $R'$  band increases extraordinarily and then becomes comparable to that of the  $\text{Cr}^{3+}$ -exciton- $\text{Cr}^{3+}$ -magnon transition.

#### IV. DISCUSSION

As mentioned in Sec. III, we have observed that a bound state appears on the lowest-energy side of the  $\text{Cr}^{3+}$  exciton coupled with  $\text{Yb}^{3+}$  spin flip in  $\text{YbCrO}_3$  and it has a strong dependence on the external magnetic field along

the  $a$  axis. In this section, we discuss the anomalous behavior of the bound state of the  $\text{Cr}^{3+}$  exciton coupled with  $\text{Yb}^{3+}$  spin flip under magnetic fields.

The  $\text{Cr}^{3+}$  excitation corresponding to the  ${}^4A_{2g} \rightarrow {}^2E_g$  transition in  $\text{YbCrO}_3$  has a negative dispersion of  $-16 \text{ cm}^{-1}$ , which reflects upon the cutoff profile at the lowest-energy side of the  $\text{Cr}^{3+}$  exciton coupled with the  $\text{Yb}^{3+}$  spin flip ( $R'$  band). From the appearance of the bound state on the low-frequency edge of the  $R'$  band, we arrive at the following concept. The  $\text{Cr}^{3+}$  excitons coupled with  $\text{Yb}^{3+}$  spin flips at the Brillouin zone edge are localized under the external magnetic field ( $\mathbf{H}_0 \parallel \mathbf{a}$ ), while the  $\text{Cr}^{3+}$  exciton coupled with  $\text{Yb}^{3+}$  spin flip at any point of the Brillouin zone except the zone edge is delocalized. In the field region where the  $\text{Cr}^{3+}$  exciton coupled with the  $\text{Yb}^{3+}$  spin flip is localized, two sharp and strong peaks due to the bound states appear, which is explained as follows. In  $\text{YbCrO}_3$ , the magnitude of the  $\text{Cr}^{3+}(i=1) - \text{Yb}^{3+}(j=5 \text{ or } 6)$  interaction is different from that of the  $\text{Cr}^{3+}(i=1) - \text{Yb}^{3+}(j=7 \text{ or } 8)$  interaction because of the orthorhombic structure. That is, the binding energy between the  $\text{Cr}^{3+}(i=1)$  exciton and the  $\text{Yb}^{3+}(j=5 \text{ or } 6)$  spin flip is different from that between the  $\text{Cr}^{3+}(i=1)$  exciton and the  $\text{Yb}^{3+}(j=7 \text{ or } 8)$  spin flip. Therefore, the bound state of the  $R'$  band in  $\text{YbCrO}_3$  splits into two components.

In the case that the bound state begins to migrate, the bound state distinguishes four  $\text{Cr}^{3+}$  sites in the unit cell. Therefore, in the process of the delocalization of the bound state, the number of the split components of the bound state changes from 2 to  $2 \times 4 = 8$ . In fact, in the field region between 2.5 and 4.5 T, the bound state of the  $R'$  band splits from 2 to 7 components. Therefore, we arrived at the following conclusion. In the region above 3 T, the zone-edge  $\text{Cr}^{3+}$  exciton coupled with  $\text{Yb}^{3+}$  spin flip begins to migrate, which reflects upon the splitting of the bound state and the significant decrease in its intensity. The splitting of the bound state is considered to be the Davydov splitting due to the intersublattice migration.

Our discovery of the Davydov splitting in the bound state is the first case for the complex elementary excitations. In connection with this, the following should be

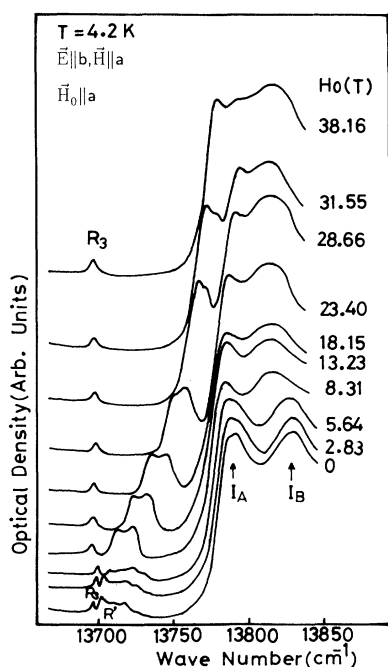


FIG. 5. Behavior of the  $R'$  band in  $\text{YbCrO}_3$  under high magnetic fields at 4.2 K (Ref. 11). The magnetic field  $\mathbf{H}_0 \parallel \mathbf{a}$ .

mentioned. The bound state of the magnon sideband corresponding to the  ${}^6A_{1g} \rightarrow {}^4E_g$  transition in  $\text{MnF}_2$  has been considered to be the Davydov split component caused by the resonance effect of the exciton-magnon pair between the nearest two sublattices. However, as mentioned in the preceding paper,<sup>5</sup> the resonance effect of the exciton-magnon pair is negligibly small and is not responsible for the appearance of the exciton-magnon bound state at zero magnetic field.

At the metamagnetic transition  $H_c$  ( $\sim 6.7$  T), the band shape of the  $R'$  band changes drastically and its bound states disappear completely for all the polarized lights. As shown in Fig. 6, the shape and width of the  $R'$  band above  $H_c$  resemble closely those of the density of states of the  $\text{Cr}^{3+}$  exciton coupled with the  $\text{Yb}^{3+}$  spin flip, which implies that the  $\text{Cr}^{3+}$  exciton coupled with the  $\text{Yb}^{3+}$  spin flip above  $H_c$  behaves as a two-particle continuum state. In the calculation of the density of states, the splitting of the  $\text{Yb}^{3+}$  ground Kramers doublet and the dispersion of the  $\text{Cr}^{3+}$  exciton are expressed as

$$E_k^{\text{Yb spin}} = \text{const} , \quad (1)$$

$$E_k^{\text{Cr exciton}} = E_0 + 2V_{11}^a \cos(ak_x) + 2V_{11}^b \cos(bk_y) \pm 8V_{13} \cos(ak_x/2) \cos(bk_y/2) \cos(ck_z/2) , \quad (2)$$

where  $E_0$  is the relevant excitation energy for the single  $\text{Cr}^{3+}$  ion,  $V_{11}^a$  and  $V_{11}^b$  represent the intrasublattice exciton transfers along the  $a$  and  $b$  axes, respectively, and  $V_{13}$  is the spin-allowed intersublattice one in the 1-3  $\text{Cr}^{3+}$  pair ( $i$  and  $j$  of  $V_{ij}$  label the inequivalent  $\text{Cr}^{3+}$  sites in a unit cell). The joint density of states of the  $\text{Cr}^{3+}$  exciton

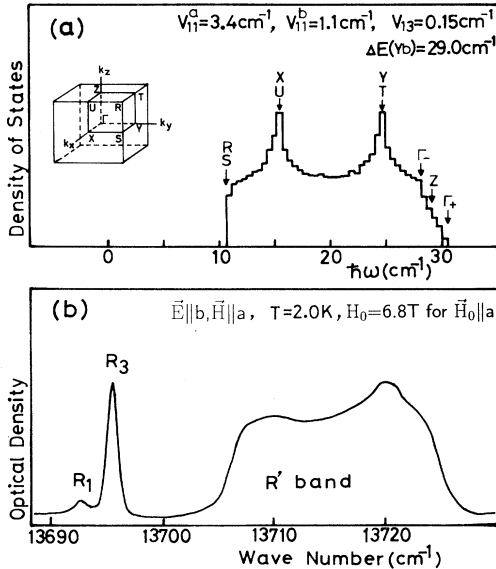


FIG. 6. (a) Joint density of states of the  $\text{Cr}^{3+}$  exciton and the  $\text{Yb}^{3+}$  spin flip in  $\text{YbCrO}_3$ . The subscripts + and - show the upper and lower branches of the exciton dispersion, respectively. The origin of the abscissa is fixed at the average energy of the  $R$  lines. The inset shows the magnetic Brillouin zone of  $\text{YbCrO}_3$  with special symmetry points marked. (b)  $R$  lines and  $R'$  band in  $\text{YbCrO}_3$  at  $H_0(\parallel a) = 6.8$  T and  $T = 2.0$  K.

and the  $\text{Yb}^{3+}$  spin flip is given by

$$\rho(\omega) = \sum_k \delta(\hbar\omega - E_k^{\text{Yb spin}} - E_{-k}^{\text{Cr exciton}}) . \quad (3)$$

$\rho(\omega)$  is calculated on a computer by counting the number of wave vectors which have the same energy, over  $50^3$  divisions throughout the first Brillouin zone.  $V_{11}^a = 3.4$   $\text{cm}^{-1}$ ,  $V_{11}^b = 1.1$   $\text{cm}^{-1}$ ,  $V_{13} = 0.15$   $\text{cm}^{-1}$ , and  $E_k^{\text{Yb spin}} = 29.0$   $\text{cm}^{-1}$  are the best-fit parameters. Using  $V_{11}^a = 3.4$   $\text{cm}^{-1}$  and  $V_{11}^b = 1.1$   $\text{cm}^{-1}$ , the exciton dispersion in the lowest substrate of the  ${}^2E_g$  state is estimated to be  $-18$   $\text{cm}^{-1}$  at  $H_0(\parallel a) = 6.8$  T.

At the metamagnetic transition, as schematically shown in Fig. 7, the weak ferromagnetic moment of the  $\text{Cr}^{3+}$  spins reverses its direction from being antiparallel to parallel to the net magnetic moment of the  $\text{Yb}^{3+}$  spins, where the antisymmetric exchange interaction between the  $\text{Cr}^{3+}$  and  $\text{Yb}^{3+}$  spins,  $D(S^{\text{Cr}} \times S^{\text{Yb}})$ , changes discontinuously in its sign and intensity. The change of the  $\text{Cr}^{3+}$ - $\text{Yb}^{3+}$  antisymmetric exchange interaction at  $H_c$  should be responsible for the drastic change of the  $R'$  band. From the fact that the bound state of the  $R'$  band vanishes completely at  $H_c$ , the following is considered. The  $\text{Cr}^{3+}$ - $\text{Yb}^{3+}$  antisymmetric exchange interaction between the  $\text{Cr}^{3+}$  exciton and the  $\text{Yb}^{3+}$  spin flip is attractive below  $H_c$ . On the contrary, its attractive force vanishes above  $H_c$ .

In the field region ( $H_0 > 25$  T), where the energy position of the  $R'$  band approaches that of the magnon sideband ( $\text{Cr}^{3+}$  exciton coupled with  $\text{Cr}^{3+}$  magnon), the intensity of the  $R'$  band increases by 1 or 2 orders of magnitude and then approaches that of the magnon sideband ( $I_A$  and  $I_B$  bands).

Figure 8(a) shows the  $\text{Yb}^{3+}$  spin-flip energy in  $\text{YbCrO}_3$  as a function of external magnetic field along the  $a$  axis, which is estimated from the  $\text{Yb}^{3+}$  absorption spectra in  $\text{YbCrO}_3$  under magnetic fields.<sup>9,13</sup> Figure 8(b) shows the density of states of the  $\text{Cr}^{3+}$  magnon in  $\text{YbCrO}_3$ , whose calculation is shown in the Appendix. As shown in Fig. 8, in the field region  $H_0 > 25$  T, the  $\text{Yb}^{3+}$  spin-flip energy approaches the  $\text{Cr}^{3+}$  magnon energy whose density of states is very high, consequently the  $\text{Yb}^{3+}$  spin-flip mode is strongly hybridized with the  $\text{Cr}^{3+}$  magnon mode, so that the noticeable increase of the intensity of the  $R'$

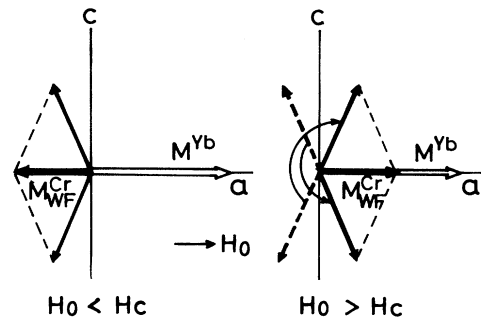


FIG. 7. Spin arrangements of  $\text{YbCrO}_3$  which are projected into the  $ac$  plane below and above the metamagnetic transition  $H_0 (= 6.7$  T).

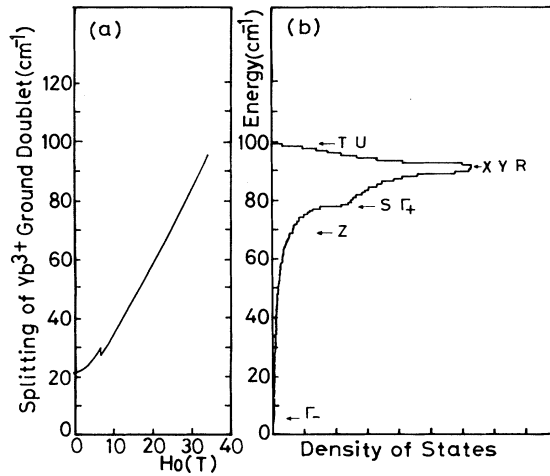


FIG. 8. (a) Splitting of the ground Kramers doublet of  $\text{Yb}^{3+}$  in  $\text{YbCrO}_3$  at 4.2 K in the external magnetic field applied along the  $a$  axis, which is estimated from the  $\text{Yb}^{3+}$  absorption spectra corresponding to the  ${}^2F_{7/2} \rightarrow {}^2F_{5/2}$  transition in  $\text{YbCrO}_3$  under high magnetic fields (Refs. 9 and 13). (b) Density of states of the  $\text{Cr}^{3+}$  magnon in  $\text{YbCrO}_3$ , where  $J_1 = -14.6 \text{ cm}^{-1}$  and  $J_2 = -1.8 \text{ cm}^{-1}$ .

band under the external magnetic field region ( $\mathbf{H}_0 \parallel \mathbf{a}$ ,  $H_0 > 25 \text{ T}$ ) is attributed to the strong hybridization of the  $\text{Yb}^{3+}$  spin-flip mode and the  $\text{Cr}^{3+}$  magnon mode. In this field region, the  $\text{Yb}^{3+}$  spin becomes Heisenberg-like and its spin-flip mode is able to migrate because of the strong hybridization between the  $\text{Yb}^{3+}$  spin-flip mode and the  $\text{Cr}^{3+}$  magnon mode.

Therefore, under high magnetic fields, the  $\text{Cr}^{3+}$  exciton coupled with the  $\text{Yb}^{3+}$  spin flip is delocalized completely, and as a result the  $R'$  band reveals the continuous spectrum of the  $\text{Cr}^{3+}$ -exciton- $\text{Yb}^{3+}$ -spin-flip dissociated states (two-particle states).

## V. CONCLUSION

We have investigated the  $\text{Cr}^{3+}$  exciton coupled with the  $\text{Yb}^{3+}$  spin flip ( $R'$  band) in  $\text{YbCrO}_3$  under external magnetic fields. In the case of  $\mathbf{H}_0 \parallel \mathbf{a}$  (along the weak ferromagnetic moment), we found that a bound state appears on the lowest energy side of the  $R'$  band and has a strong dependence on external magnetic field, which is summarized as follows.

(i)  $H_0 < 3.0 \text{ T}$ . In this field region, sharp and strong peaks typical of bound states appear on the low-frequency edge of the  $R'$  band. The number of the bound states is 2, which is attributed to two kinds of binding energies between the  $\text{Cr}^{3+}$  exciton and the  $\text{Yb}^{3+}$  spin flip because of the orthorhombic structure. The  $\text{Cr}^{3+}$  excitons coupled with  $\text{Yb}^{3+}$  spin flips at the Brillouin zone edge are localized, while the zone-inside ones are delocalized.

(ii)  $3.0 \text{ T} < H_0 < H_c (6.7 \text{ T})$ . In this field region, the bound state of the  $R'$  band splits into seven peaks and their intensities decrease significantly. The splitting of the bound state is considered to be the Davydov splitting due to the intersublattice migration.

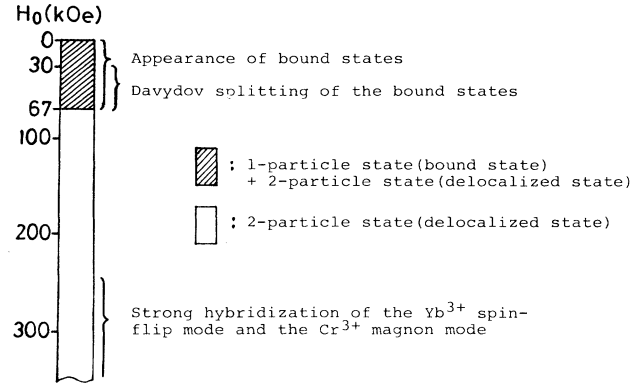


FIG. 9. Profiles of the  $\text{Cr}^{3+}$  exciton coupled with  $\text{Yb}^{3+}$  spin flip in  $\text{YbCrO}_3$  under magnetic fields ( $\mathbf{H}_0 \parallel \mathbf{a}$ ).

(iii)  $H_0 = H_c (6.7 \text{ T})$ . At the metamagnetic transition  $H_c$ , where the weak ferromagnetic moment of the  $\text{Cr}^{3+}$  spins reverses its direction from being antiparallel to parallel to the net magnetic moment of the  $\text{Yb}^{3+}$  spins, the bound states disappear completely for all the polarized lights and the shape and energy position of the  $R'$  band change drastically, which is attributed to the discontinuous change of the antisymmetric exchange interaction between the  $\text{Cr}^{3+}$  and  $\text{Yb}^{3+}$  spins. This antisymmetric exchange interaction between the  $\text{Cr}^{3+}$  excitons and the  $\text{Yb}^{3+}$  spin flips at the zone boundary is attractive below  $H_c$ , however, its attractive force vanishes above  $H_c$ .

(iv)  $H_0 > H_c$ . In this field region, the shape of the  $R'$  band resembles closely the density of states of the  $\text{Cr}^{3+}$  exciton coupled with the  $\text{Yb}^{3+}$  spin flip, which implies that the  $\text{Cr}^{3+}$  exciton coupled with the  $\text{Yb}^{3+}$  spin flip behaves as a two-particle continuous state above  $H_c$ .

In the region above about 25 T, the intensity of the  $R'$  band increases by 1 or 2 orders of magnitude and then approaches that of the  $\text{Cr}^{3+}$  exciton coupled with the  $\text{Cr}^{3+}$  magnon, which is due to the strong hybridization of the  $\text{Yb}^{3+}$  spin-flip mode and the  $\text{Cr}^{3+}$  magnon mode.

The behavior of the  $\text{Cr}^{3+}$  exciton coupled with the  $\text{Yb}^{3+}$  spin flip in  $\text{YbCrO}_3$  under the magnetic field  $\mathbf{H}_0 \parallel \mathbf{a}$  is summarized in Fig. 9.

In connection with the  $R'$  band in  $\text{YbCrO}_3$ , it is worth noting that the behavior of the bound state of the  $\text{Cr}^{3+}$  exciton coupled with the  $\text{Yb}^{3+}$  spin flip in  $\text{YbCrO}_3$  resembles closely that of the bound state (vibron) of the vibronic exciton in molecular crystals such as naphthalene.<sup>14</sup> It can be correspondence:  $\text{Cr}^{3+}$  exciton  $\leftrightarrow$  molecular exciton,  $\text{Yb}^{3+}$  spin flip  $\leftrightarrow$  intramolecular vibration. In general, the spin-flip mode of the Ising-like spin and the intramolecular vibration have no energy dispersion. In the case of the vibronic exciton in molecular crystals, the attractive force between the exciton and the intramolecular vibration, responsible for the appearance of the vibron, is the second-order exciton-phonon interaction.<sup>14</sup> On the other hand, the attractive force between the  $\text{Cr}^{3+}$  exciton and the  $\text{Yb}^{3+}$  spin flip in  $\text{YbCrO}_3$  is considered to be the strong antisymmetric exchange interaction between the  $\text{Cr}^{3+}$  and  $\text{Yb}^{3+}$  spins.

## ACKNOWLEDGMENT

The author wishes to thank Professor K. Tsushima of Kyushu Institute of Technology for valuable suggestions and kindly supplying the crystal.

$$E_k^{\text{ac}} = S \{ [\gamma_{12}(0) + \gamma_{14}(0) - \gamma_{13}(0) + \gamma_{13}(k) - \gamma_{11}^x(0) + \gamma_{11}^x(k) - \gamma_{11}^y(0) + \gamma_{11}^y(k)]^2 - [\gamma_{12}(k) + \gamma_{14}(k)]^2 \}^{1/2}, \quad (\text{A1})$$

$$E_k^{\text{op}} = S \{ [\gamma_{12}(0) + \gamma_{14}(0) - \gamma_{13}(0) - \gamma_{13}(k) - \gamma_{11}^x(0) + \gamma_{11}^x(k) - \gamma_{11}^y(0) + \gamma_{11}^y(k)]^2 - [\gamma_{12}(k) - \gamma_{14}(k)]^2 \}^{1/2}, \quad (\text{A2})$$

where

$$\begin{aligned} \gamma_{12}(k) &= 2J_{12} \cos(ck_z/2), \\ \gamma_{14}(k) &= 2J_{14} \cos(ak_x/2) \cos(bk_y/2), \\ \gamma_{13}(k) &= 8J_{13} \cos(ak_x/2) \cos(bk_y/2) \cos(ck_z/2), \\ \gamma_{11}^x(k) &= 2J_{11}^x \cos(ak_x), \\ \gamma_{11}^y(k) &= 2J_{11}^y \cos(bk_y). \end{aligned} \quad (\text{A3})$$

$E_k^{\text{ac}}$  and  $E_k^{\text{op}}$  denote the acoustic and optical branches, respectively.  $J_{ij}$  represents the exchange interaction in the  $i$ - $j$   $\text{Cr}^{3+}$  pair ( $i$  and  $j$  label the inequivalent  $\text{Cr}^{3+}$  sites in a unit cell), and  $J_{11}^a$  and  $J_{11}^b$  represent the intrasublattice exchange interaction along the  $a$  and  $b$  axes, respectively.

The exchange interaction constants  $J_1$  and  $J_2$  are defined as

$$J_1 = J_{12} = J_{14}, \quad J_2 = J_{11}^x = J_{11}^y = J_{13}. \quad (\text{A4})$$

From the magnetic susceptibility measurement, the

## APPENDIX

In the case of the four-sublattice system, the magnon spectrum consists of two branches. The dispersion of the  $\text{Cr}^{3+}$  magnon in rare-earth orthochromite  $R\text{CrO}_3$  is expressed as<sup>15</sup>

asymptotic Weiss temperature  $\theta$  has been estimated to be  $-230$  K.<sup>16</sup> By using  $T_{N1} = 118$  K and  $\theta = -230$  K,  $J_1$  and  $J_2$  are estimated to be  $-14.6$  and  $-1.8$  cm<sup>-1</sup>, respectively, from the molecular field relations  $\theta = S(S+1)(6J_1 + 12J_2)/3k$  and  $T_{N1} = S(S+1)(-6J_1 + 12J_2)/3k$ .

The density of states of the  $\text{Cr}^{3+}$  magnon in  $\text{YbCrO}_3$  is calculated on a computer by counting the number of wave vectors which have the same energy, over 50<sup>3</sup> divisions throughout the first Brillouin zone, which is shown in Fig. 8(b). In connection with this calculation, the following should be mentioned. In the case of rare-earth orthochromite  $R\text{CrO}_3$ , the density of states of the  $\text{Cr}^{3+}$  magnon in  $\text{YCrO}_3$  has already been calculated by van der Ziel and Van Uitert.<sup>17</sup> The density of states of the  $\text{Cr}^{3+}$  magnon in  $\text{YCrO}_3$  consists of two peaks, which is quite different from that in  $\text{YbCrO}_3$ . This discrepancy is attributed to a mistake in the energy dispersion of the optical magnon mode calculated by van der Ziel and Van Uitert. The density of states of the  $\text{Cr}^{3+}$  magnon in  $\text{YCrO}_3$  calculated by using Eqs. (A1) and (A2) is very similar to that in  $\text{YbCrO}_3$ .

<sup>1</sup>R. S. Meltzer, M. Y. Chen, M. Lowe-Pariseau, and D. S. McClure, Phys. Rev. Lett. **21**, 913 (1968).

<sup>2</sup>R. S. Meltzer, M. Lowe, and D. S. McClure, Phys. Rev. **180**, 561 (1969).

<sup>3</sup>N. Kojima and I. Tsujikawa, J. Phys. (Paris) Colloq. **49**, C8-897 (1988).

<sup>4</sup>N. Kojima (unpublished).

<sup>5</sup>N. Kojima, M. Kawarazaki, I. Mogi, M. Takeda, G. Kido, and Y. Nakagawa, preceding paper, Phys. Rev. B **47**, 15 086 (1993).

<sup>6</sup>S. Quezel-Ambrunaz and M. Mareschal, Bull. Soc. Fr. Mineral. Cristallogr. **LXXXVI**, 204 (1963).

<sup>7</sup>S. Shtrikman, B. M. Wanklyn, and I. Yaeger, Int. J. Magn. **1**, 327 (1971).

<sup>8</sup>E. F. Bertaut, in *Magnetism III*, edited by G. T. Rado and H. Suhl (Academic, New York, 1963), p. 149.

<sup>9</sup>N. Kojima, K. Tsushima, and I. Tsujikawa, J. Phys. Soc. Jpn. **49**, 1449 (1980).

<sup>10</sup>N. Kojima, K. Aoyagi, K. Tsushima, I. Tsujikawa, and S. Sugano, J. Phys. Soc. Jpn. **49**, 1463 (1980).

<sup>11</sup>N. Kojima, I. Tsujikawa, H. Hori, H. Nishimura, and M. Date, J. Phys. Soc. Jpn. **53**, 2875 (1984).

<sup>12</sup>N. Kojima, K. Tsushima, S. Kurita, and I. Tsujikawa, J. Phys. Soc. Jpn. **49**, 1456 (1980).

<sup>13</sup>N. Kojima, M. Kawarazaki, I. Mogi, M. Takeda, G. Kido, and Y. Nakagawa (unpublished).

<sup>14</sup>V. L. Broude, E. I. Rashba, and E. F. Sheka, *Spectroscopy of Molecular Excitons* (Springer-Verlag, Berlin, 1985), p. 206.

<sup>15</sup>S. M. Shapiro, J. D. Axe, and J. P. Remeika, Phys. Rev. B **10**, 2014 (1974).

<sup>16</sup>J. B. Goodenough and J. M. Longo, in *Magnetic Oxides and Related Compounds*, Landolt-Börnstein, New Series, Group III, Vol. 4a, edited by K. H. Hellwege (Springer-Verlag, Berlin, 1969), p. 228.

<sup>17</sup>J. P. van der Ziel and L. G. Van Uitert, Phys. Rev. **179**, 343 (1969).